Dimensional Analysis Approach for Simultaneous Estimation of Electrical Conductivity and Lift-Off in Eddy Current Testing

Alessandro Sardellitti, *Member, IEEE*, Vincenzo Mottola, *Member, IEEE*, Filippo Milano, *Member, IEEE*, Marco Laracca, *Member, IEEE*, Luigi Ferrigno, *Senior Member, IEEE*, and Antonello Tamburrino, *Senior Member, IEEE*

***Abstract*—Accurate estimation of electrical conductivity and lift-off is crucial in eddy current testing (ECT) to assess material properties and ensure inspection accuracy. Traditional methods often struggle with computational complexity, parameter dependency, and limited applicability to real-time scenarios. In this article, we propose an innovative methodology based on dimensional analysis and Buckingham's π theorem to simultaneously estimate electrical conductivity and lift-off with reduced computational effort. The methodology reformulates the inversion problem in a dimensionless form, significantly simplifying the inverse estimation process. The proposed solution is based on a single or multifrequency strategy, allowing efficient real-time processing and ensuring good accuracy. The experimental campaign shows that the proposed methodology generally achieves errors lower than 3% for electrical conductivity and 2% for lift-off, confirming the robustness and repeatability of the method over different materials and frequency ranges. Compared to conventional techniques, the proposed methodology provides a computationally efficient and scalable solution, which makes it suitable for online and real-time industrial applications.**

***Index Terms*—Dimensional analysis, eddy current testing (ECT), electrical conductivity estimation, lift-off estimation, nondestructive testing, simultaneous estimation.**

I. Introduction

IN THE context of materials analysis and industrial manufacturing, the accurate measurement of material properties is crucial to ensure product quality, structural integrity, and functional performance. Measurement techniques can be broadly classified into destructive and nondestructive testing (NDT) methods, and further into contact-based and contactless approaches. Among these measurement techniques, NDT methods are particularly attractive because they allow property estimation or defect detection without altering or damaging the component under inspection [1], [2], [3].

Eddy current testing (ECT) differs from other NDT techniques in its ability to perform rapid, localized, and noncontact measurements on metallic materials. It is widely used in industry thanks to several advantages: high sensitivity to both surface and subsurface inspections, low cost, easy integration into automated measurement systems, and applicability to both defect/corrosion detection and material properties estimation [4], [5], [6], [7], [8].

This article focuses on the estimation of two key quantities of coated or uncoated conductive materials: electrical conductivity and lift-off (distance between the probe and the material surface). On the one hand, electrical conductivity provides valuable information on the composition, mechanical properties, and thermal process history of the conductive sample [8], [9], [10], [11]. On the other hand, lift-off is a key parameter for assessing the thickness and quality of nonconductive coatings and painting processes, and a critical factor that strongly influences any kind of ECT measurement where unknown lift-off variations can affect the sensitivity and accuracy of the results [12], [13].

When the interest is focused on the estimation of electrical conductivity and/or lift-off, different solutions have been proposed to mitigate the mutual influence between these two parameters. Considering electrical conductivity measurements, several methods that are insensitive to lift-off can be found in the literature [5], [14], [15], [16]. For example, in [16], a sweep-frequency ECT approach uses the cross-over frequency of the mutual inductance to infer conductivity while applying compensation to reduce the lift-off effect, lowering the relative error from 20.4% to 3.2%. In [5], the authors propose a logarithmic relationship between phase and conductivity, using a fixed lift-off reference to compensate for lift-off influence, achieving errors within 3%. These lift-off-insensitive methods are limited by the capability to only compensate for the lift-off without allowing for its valuable estimation. In contrast to these techniques, various alternative methods have been proposed, mainly based on simultaneous estimation of both electrical conductivity and lift-off [4], [17], [18], [19]. These approaches offer improved flexibility, as they enable parameter

Received 9 September 2025; revised 4 January 2026; accepted 18 January 2026. Date of publication 6 February 2026; date of current version 24 February 2026. The Associate Editor coordinating the review process was Dr. Maryam Shamgholi. *(Corresponding author: Alessandro Sardellitti.)*

Alessandro Sardellitti is with the Department of Engineering and Science, Universitas Mercatorum, 00186 Rome, Italy (e-mail: alessandro.sardellitti@unimercatorum.it).

Vincenzo Mottola, Filippo Milano, Luigi Ferrigno, and Antonello Tamburrino are with the Department of Electrical and Information Engineering, University of Cassino and Southern Lazio, 03043 Cassino, Italy (e-mail: vincenzo.mottola@unicas.it; filippo.milano@unicas.it; ferrigno@unicas.it; tamburrino@unicas.it).

Marco Laracca is with the Department of Electrical and Energy Engineering, Sapienza University of Rome, 00184 Rome, Italy (e-mail: marco.laracca@uniroma1.it).

Digital Object Identifier 10.1109/TIM.2026.3661690

estimation without requiring prior knowledge of other material properties, thus extending their applicability to more complex or variable inspection scenarios. In [4], the authors present a portable embedded measurement system for the contactless estimation of electrical conductivity and lift-off. The system utilizes an absolute probe with compensation to measure the in-phase and in-quadrature components of the probe voltage. The polynomial relationships used in the adopted model, defined by 11 coefficients for conductivity and ten for lift-off, are determined during a prior calibration phase using measurements on reference samples at a single operating frequency. Although this approach simplifies the measurement process for the end user, it constrains the accuracy and applicability of the system to calibrated conditions, including a limited lift-off interval and minimum sample thickness requirements. Any change in frequency, probe configuration, or extension of the material set would require a complete recalibration involving multiple measurements on known standards. Lu et al. [17] introduced the concept of dual-frequency linearity between sensor lift-off and the change in inductance in eddy current (EC) measurements. They have developed an algorithm that exploits this linearity to accurately reconstruct lift-off values up to 20 mm. Furthermore, an iterative inverse solver (a modified Newton–Raphson method) was used to refine the reconstruction of sample properties, achieving notably low errors, even for larger sensor lift-offs. Despite good performance, the Newton–Raphson method can lead to false solutions or increased computational cost, particularly when applied to real-time or inline applications. In [18], a new ECT method with a material-independent model for coupled-parameter estimation has been proposed. In this case, good performance was obtained in estimating electrical conductivity, but tests were carried out only for low electrical conductivities (0.56–1.92 MS/m), limiting its applicability to a wider range of materials. Huang et al. [19] proposed a method that integrates sweep-frequency EC measurements with machine learning to estimate the permeability, conductivity, thickness, and lift-off of conductive plates. Although the method achieves good accuracy (within 3.5%), its applicability for inline and real-time applications is limited due to the requirement of estimating five parameters across both low- and high-driving frequency ranges.

These works highlight that accurate and fast estimation of electrical conductivity and lift-off continues to be an open issue, with ongoing efforts in the scientific community to develop methods to improve accuracy, robustness, and applicability to different materials and field scenarios. Further advancements are required to address limitations in existing techniques, particularly for online and real-time applications, as well as for materials that exhibit a wide range of conductivity and lift-off conditions.

In this article, we present a comprehensive analysis of the application of dimensional analysis, with a particular focus on Buckingham's π theorem [20], for simultaneous estimation of the electrical conductivity of conductive samples and the lift-off. Starting from the recent introduction of this methodology for ECT thickness measurement [21] and for the simultaneous estimation of electrical conductivity and thickness [22], this work extends our preliminary numerical study presented in [23], which provided initial evidence of the potential of Buckingham's π theorem for the simultaneous estimation of electrical conductivity and lift-off in non-magnetic conductive materials.

Compared to methods already proposed in the scientific literature, the methodology proposed in this article offers several advantages. Specifically, Buckingham's π theorem makes it possible to reduce the number of independent variables affecting the measured quantity by combining the original variables in the so-called dimensional groups or π-groups, based on the concept that physics is independent of the choice of units. This methodology reduces the computational complexity of the problem, without introducing any approximation of the underlying physics, overcoming the limits on the range on lift-off values found in various methods proposed in the literature [13], [24].

Finally, the proposed method allows the user to balance the tradeoff between estimation accuracy and the measurement time. Depending on the specific requirements of the application, it can be implemented using a single-frequency approach for fast measurements or a multifrequency strategy to improve accuracy. In both cases, real-time operations are supported.

The article is organized as follows. Section II provides an overview of Buckingham's π theorem and its customization to the simultaneous estimation of electrical conductivity and lift-off via ECT. Section III describes the experimental setup and the cases of interest. The experimental results are presented in Section IV. Finally, conclusions are drawn in Section V.

II. Dimensional Analysis and Estimation Method

This section introduces the theoretical background and methodological framework adopted for the simultaneous estimation of electrical conductivity and lift-off in ECT. The problem is reformulated using dimensional analysis and Buckingham's π theorem, allowing for a simplified and efficient estimation process. To improve clarity and readability, the section is divided into two subsections: 1) the dimensional analysis principles applied to ECT and 2) the proposed estimation approach based on dimensionless variables.

A. Dimensional Analysis in ECT

In ECT methods, an EC probe (ECP) typically consists of an excitation coil, which generates a time-varying magnetic field, inducing ECs in a conductive material, and a receiver coil or a sensor, which detects the response magnetic field. Various probe configurations can be employed, including single or multiple coils for excitation and measurement [12], [22], or setups using a single excitation coil with a magnetic field sensor [7], [25]. Both single-frequency and multifrequency acquisition strategies can be used, measuring quantities such as magnetic field variation, self-impedance, or mutual impedance.

Across these configurations, dimensional analysis and in particular Buckingham's π theorem, provides a robust framework to reduce the complexity of physical models by expressing them in terms of dimensionless variables. Without loss of generality, this article focuses on multiple coaxial coils,

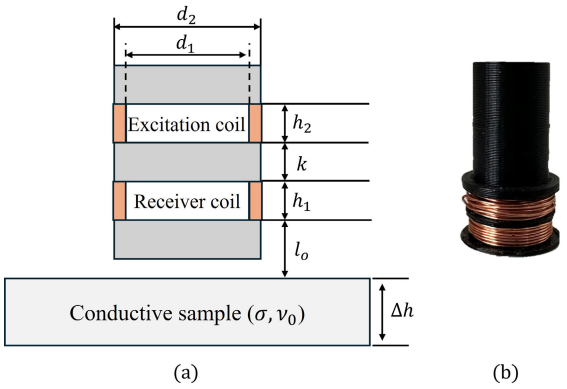

Fig. 1. Adopted coaxial ECP. (a) Schematic representation. (b) Actual pictures.

TABLE I
π-GROUPS FOR THE CONSIDERED EC PROBLEM [22], [23]

$\bar{\pi}_1 = \frac{\Delta \dot{Z}_m \nu_0}{N_1 N_2 2\pi f D}$	$\pi_2 = D\sqrt{\frac{\pi f \sigma}{\nu_0}}$	$\pi_3 = \frac{\Delta h}{D}$
$\pi_4 = \frac{l_o}{D}$	$\pi_5 = \mathbf{t}$	

as shown in Fig. 1. The mutual impedance ($\dot{Z}_m$) between the coils is the measured quantity.

Starting from $\dot{Z}_m$, the mutual impedance variation $\Delta\dot{Z}_m$ is defined as the difference between the impedance measured on the conductive sample and that measured in air. The impedance variation $\Delta\dot{Z}_m$ depends on several geometric and physical parameters, and can be expressed as

$$\Delta\dot{Z}_m = F\left(f, \sigma, \nu_0, \Delta h, D, \mathbf{t}, l_o, N_1, N_2\right) \tag{1}$$

where N_1 and N_2 are the number of turns in the driving and receiver coils, respectively. The driving frequency is f. The sample's properties from the ECT perspective are its electrical conductivity σ, magnetic reluctance ν_0 (equal to that of the vacuum for nonmagnetic materials), and the thickness Δh. The geometry of the probe is characterized by (d_1, d_2, h_1, h_2, k) (see Fig. 1). Let D be a representative size of the probe (equal to $d_2/2$ in this case), and the geometrical parameters form a dimensionless vector $\mathbf{t} = (d_1/D, h_1/D, h_2/D, k/D)$. Hereafter, l_o is the lift-off of the probe.

Similar functional relationships can be derived for other ECP configurations, illustrating the inherent complexity of physical models in their dimensional representation. The large number of variables involved increases the computational demand, making a method incompatible with the real-time requirements for online and inline applications.

A powerful tool of dimensional analysis is Buckingham's π theorem, which simplifies this complexity by reducing the number of independent variables [20], without the need for any approximation. Specifically, it states that any physical relationship initially dependent on n dimensional quantities can be reformulated in terms of $n - z$ dimensionless quantities, known as π-groups, where z represents the number of fundamental dimensions needed to describe the system.

Tamburrino et al. [22] and Sardellitti et al. [23] have successfully applied Buckingham's π theorem to (1), yielding the π-groups listed in Table I and the dimensionless reformulation shown in (2).

TABLE II
NUMERICAL EVALUATION PARAMETERS AND CORRESPONDING DIMENSIONLESS RANGES

Parameter	Min:Step:Max values	Corresponding π group range
σ	25 MS/m (fixed)	$\pi_2 \in [0.547,\ 34.601]$
f	100 : 100 : 400000 Hz	
Δh	0.5 : 0.05 : 6 mm	$\pi_3 \in [0.091,\ 1.089]$
l_0	0.05 : 0.05 : 4.5 mm	$\pi_4 \in [0.0091,\ 0.8171]$
t	fixed (see Table III)	$\pi_5 = \text{const.}$

Equation (2) reveals the dependence of the mutual impedance variation on dimensionless variables, allowing the problem to be represented in a smaller dimensional space

$$\bar{\pi}_1 = r\left(\pi_2, \pi_3, \pi_4, \pi_5\right). \tag{2}$$

B. Proposed Estimation Method

The proposed estimation method relies on three key stages: 1) the generation, in a numerical environment, of level curves in dimensionless planes; 2) the selection of proper level curves, given the experimental measurements; and 3) the solution of the inverse problem (i.e., estimation of both electrical conductivity and lift-off).

1) Level Curves: The effectiveness of the introduction of level curves in the framework of the solution of ECT problems was initially recognized and proposed in [21], [22], and [23].

Before introducing the level curves, it is worth noting that (2) can be simplified, depending on the specific operating conditions. First, if the ECP geometry is prescribed, the dimensionless group π_5 is constant. Similarly, if the thickness Δh is fixed, then π_3 is constant. In this work, both the ECT probe and the thickness of the metallic specimen are known, thus the dimensionless function r of (2) reduces to a function of only two dimensionless variables

$$\bar{\pi}_1 = G\left(\pi_2, \pi_4\right) \tag{3}$$

where it is understood that π_3 and π_5 are fixed parameters. The unknown pair (π_2, π_4) varies in the dimensionless parameter space $\mathbb{P} = (0, +\infty) \times (0, +\infty)$.

Since $\bar{\pi}_1$ is a complex-valued quantity, it can be represented through distinct features such as the real $\mathrm{Re}\{\bar{\pi}_1\}$ and the imaginary $\mathrm{Im}\{\bar{\pi}_1\}$ parts, or the magnitude $|\bar{\pi}_1|$ and the phase $\angle\bar{\pi}_1$. For each of these features, a family of level curves (iso-value curves) in $\mathbb{P}$ can be introduced. A level curve in $\mathbb{P}$ represents the locus of the points where a selected feature is constant. Since the dimension of the parameter space $\mathbb{P}$ is two, it can be represented via a plane, and thus, the level curves are curves in a plane, as shown in Fig. 2 for the four key features (Re, Im, $|\ |$, and $\angle$) considered in this work.

For this specific problem, the generation of the level curves is carried out numerically using the semi-analytical model of Dodd and Deeds [26], which was applied to compute $\Delta\dot{Z}_m$ as a function of the physical quantities listed in Table II, and the geometry of the ECP described in Table III. The generality of the method is given by the fact that level curves can be easily

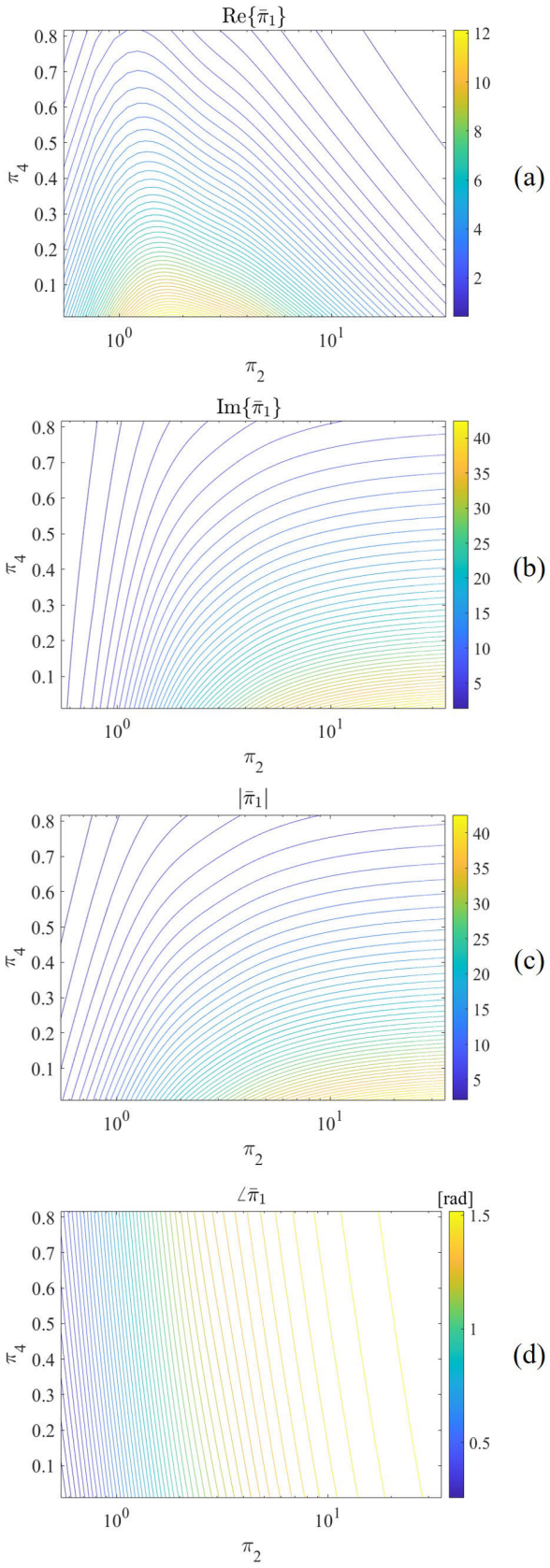

Fig. 2. Level curves of $\bar{\pi}_1$. (a) Re$\{\bar{\pi}_1\}$, (b) Im$\{\bar{\pi}_1\}$, (c) $|\bar{\pi}_1|$, and (d) $\angle\bar{\pi}_1$ obtained from the parameters described in Table II. The maps were generated by varying π_2 and π_4 while keeping π_3 fixed.

generated with other simulation tools and/or for other probe configurations and/or for other geometries.

TABLE III
GEOMETRICAL DIMENSIONS OF THE ADOPTED ECP

Parameter	Value
$h_1 = h_2$	2.60 mm
k	0.76 mm
d_1	10.00 mm
d_2	11.01 mm
l_0	0.41 mm
$N_1 = N_2$	12

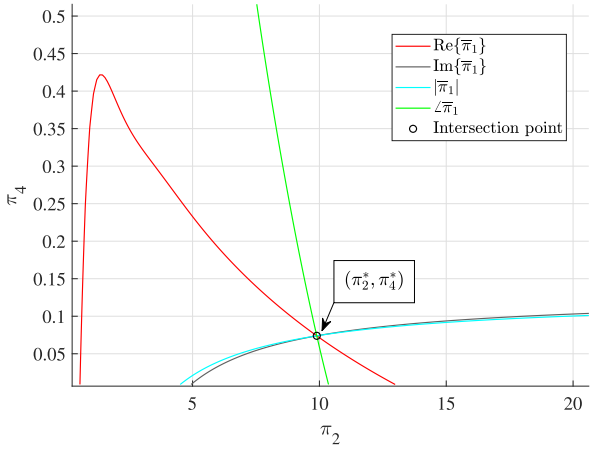

Fig. 3. Intersection of level curves determining the solution (π_2^*, π_4^*), obtained using a single driving frequency.

The dimensional parameters, shown in Table II, were varied within suitable operating ranges to create a database consistent with the typical values found in various application fields, such as ECT and industrial contexts. To explore the representative electrical conductivity ranges of conductive materials (e.g., copper, aluminum, and bronze) and considering the frequencies available from a typical impedance analyzer, the driving frequency range was accordingly defined. From these considerations, the resulting range for π_2 was obtained. Similar reasoning was applied to the selection of thickness and lift-off, leading to the definition of the ranges for π_3 and π_4.

It is important to note that the electrical conductivity σ was kept constant during the numerical campaign. Since the dimensionless group π_2 depends on the product $\sigma \cdot f$, the same range of π_2 values could be obtained either by varying σ or f. This reduction in independent variables is another key advantage of dimensional analysis, as it reduces computational cost while preserving the generality of the model.

2) Selection of the Level Curve: In the second phase, the mutual impedance variation $\Delta\dot{Z}_m$ is experimentally measured at a defined driving frequency f. From the measured $\Delta\dot{Z}_m$, the corresponding value of $\bar{\pi}_1$ is evaluated, and its features are extracted. The values of each feature are then used to select a specific level curve in the (π_2, π_4) plane.

3) Parameter Estimate: In this last phase, the selected level curves are used to solve the inverse problem (i.e., the estimation of both the electrical conductivity and lift-off). For the simultaneous estimation of these two parameters, the selected level curves corresponding to at least two of the four

features are combined. Specifically, their intersection provides the estimate of the electrical conductivity and the lift-off, in terms of dimensionless groups π_2 and π_4, respectively (see Fig. 3). The use of more than two features can be used to increase the robustness of the estimation. The intersection point (π_2^*, π_4^*), shown in Fig. 3, allows to estimate the unknown parameters as follows:

$$\sigma^* = \frac{\nu_0}{\pi f} \cdot \left(\frac{\pi_2^*}{D}\right)^2 \tag{4}$$

$$l_o^* = D \cdot \pi_4^*. \tag{5}$$

Equations (4) and (5) were obtained by inverting the definitions of π_2 and π_4 reported in Table I, in order to express the electrical conductivity and lift-off in their dimensional form.

It is important to note that, in experimental measurements, when more than two features are used, multiple intersections may occur due to measurement noise. In such cases, central tendency parameters (e.g., mean, median, or mode) can be employed to obtain a unique solution. In this work, the mean value of the intersections is used to determine the final estimate.

While this approach is effective using a single driving frequency, it can be naturally extended to a multifrequency framework [see Fig. 4(a)]. In this case, multiple impedance measurements are acquired at different frequencies, resulting in a set of $\bar{\pi}_{1,i}$ values and corresponding intersection points $(\pi_{2,i}^*, \pi_{4,i}^*)$ in the (π_2, π_4) plane. These points shift along the π_2 axis (which depends on f) but, when bringing back the level curves onto the dimensional plane (σ, l_o), they show a single intersection point corresponding to the electrical conductivity σ^* and the lift-off l_o^* [see Fig. 4(b)]. This technique has been introduced in [22] to retrieve the electrical conductivity and the thickness of a metallic plate. Moreover, because of the noise, the intersection may spread in a neighborhood of the solution. In this case, they can be analyzed using statistical tools (e.g., averaging and clustering) to improve the estimate of σ^* and l_o^*.

In summary, the proposed methodology supports both single- and multifrequency implementations. The single-frequency configuration is particularly attractive for fast and low-complexity applications, such as real-time inline inspections. The multifrequency version, on the other hand, offers an effective means to enhance accuracy and robustness when required by the specific use case.

Finally, a relevant potentiality of the proposed method is given by the possibility to make the simultaneous estimation of electrical conductivity and lift-off without any a-priory information about the sample thickness Δh. In fact, the analysis conducted in [22] on the dimensionless planes $(\pi_2 - \pi_3)$ have demonstrated that there are some conditions for which the level curves are independent by Δh. In particular, when the product $\pi_2 \cdot \pi_3 \geq 3$, the level curves tend to become vertical (see [22]), indicating that $\bar{\pi}_1$ becomes practically insensitive by π_3 (so by Δh). From a physical point of view, this condition corresponds to a regime in which the skin depth $\delta = 1/(\pi f \sigma / \nu_0)^{1/2}$ is at least three times smaller than the sample thickness Δh. In this regime, mutual impedance measurements are no longer sensitive to thickness variations.

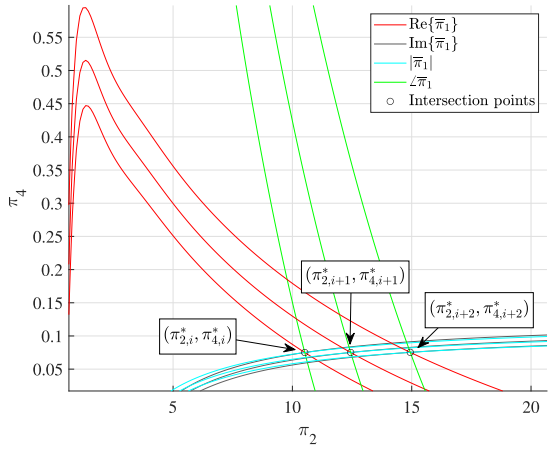

(a)

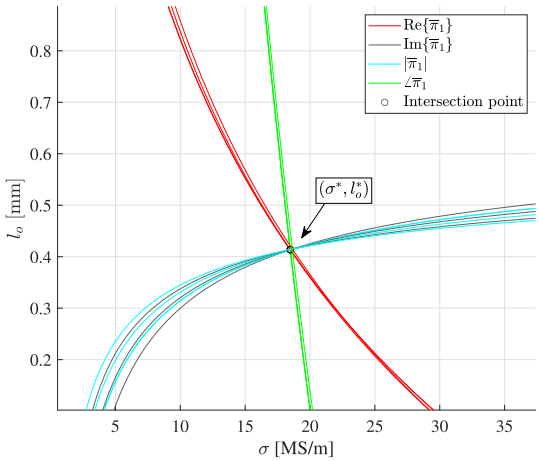

(b)

Fig. 4. Intersections of level curves determining the solutions obtained using multiple driving frequencies (a) $(\pi_{2,i}^*, \pi_{4,i}^*)$ from dimensionless plane and (b) (σ^*, l_o^*) from dimensional plane.

III. Experimental Validation

In this section, the experimental setup, the considered case studies, and the proposed measurement procedure are described.

A. Experimental Setup and Description of Considered Case Studies

The experimental setup adopted in this work is shown in Fig. 5. Specifically, Fig. 5(a) presents the block diagram representation, while Fig. 5(b) illustrates the physical implementation of the experimental setup, including the ECP placement during the test and the analyzed samples. The experimental setup consists of a GW-Instek 8000G impedance analyzer [27], interfaced to a PC via the IEEE-488 communication protocol. The impedance analyzer operates in a slow acquisition mode to ensure high measurement accuracy. Impedance measurements have been performed using the series R–L model configuration. The ECP, represented in

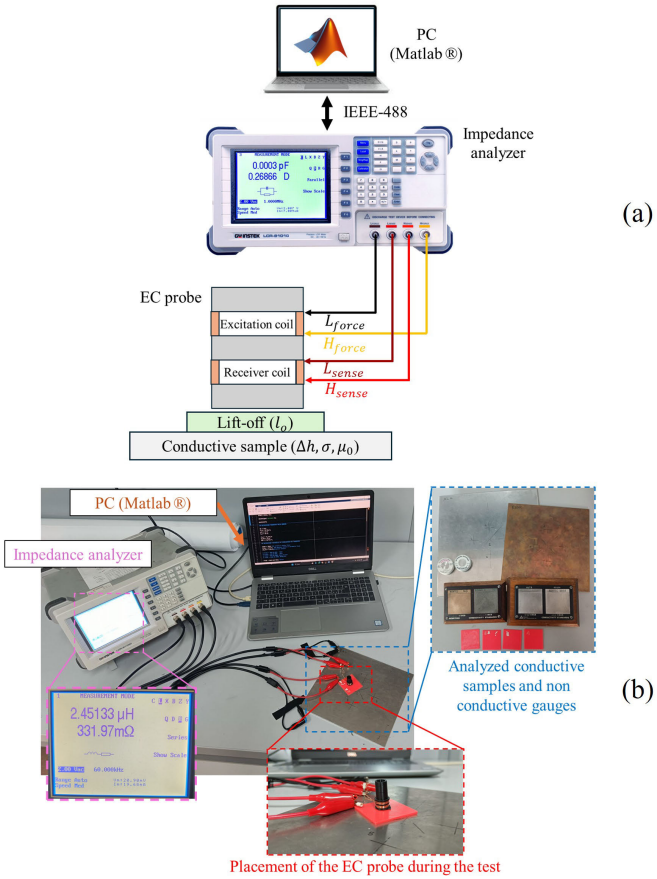

Fig. 5. Adopted experimental setup (a) block diagram representation and (b) physical implementation of the experimental setup.

TABLE IV
ELECTRICAL CONDUCTIVITY AND DIMENSIONAL PARAMETER OF THE ANALYZED SAMPLES

Name code	Alloy	Electrical conductivity (σ_a) [MS/m]	Thickness [mm]
M_1	Aluminum Bronze	5.28	6
M_2	Phosphor Bronze	11.11	6
M_3	Aluminium (7075-T6)	18.33	11
M_4	Aluminium (2014A-T6)	23.32	6
M_5	Aluminium (6082-T6)	27.80	11
M_6	Aluminium (AW-1050A)	34.93	4
M_7	Copper	58.05	1
M_8	Aluminium (5083)	16.36	6

Fig. 1, is adopted for all tests and its geometric parameters are described in Table III.

The experimental tests have been carried out on eight certified conductive samples with electrical conductivities ranging from 5.28 to 58.05 MS/m, as detailed in Table IV. The reference electrical conductivity values of the certified samples have been further verified through measurements conducted using a calibrated electrical conductivity meter [28].

Additionally, the experimental tests were performed at varying lift-off values, ranging from 0.4 to 2.3 mm, using a nonconductive gauges with different thicknesses measured via a digital micrometer. The lift-off values and corresponding measurement uncertainties were estimated by combining the statistical variability of repeated micrometer measurements with the instrument's accuracy. Accordingly, the lift-off values are reported in Table V as the mean values along with their associated measurement uncertainties.

TABLE V
ADOPTED LIFT-OFF VALUES DURING THE EXPERIMENTAL TESTS

Name code	Lift-off value (lo_a) [mm]
lo_1	0.408 ± 0.010
lo_2	0.902 ± 0.013
lo_3	1.440 ± 0.015
lo_4	1.762 ± 0.012
lo_5	2.271 ± 0.010

Measurements were carried out at driving frequencies ranging from 50 to 70 kHz, with 1 kHz step. Some details are needed to explain the selection of this frequency span. First, as described in Section II, the proposed method can be used as single- or multiple-frequency solution. So, the choice of making the experimental tests at different driving frequencies ensure a sufficiently dense characterization of the proposed method for both solutions. As far as the selection of the frequency range, it was chosen to satisfy the condition $\pi_2 \cdot \pi_3 > 3$, as discussed in Section II, which ensures the independence of the estimation method from the value of the sample thickness.

The entire measurement workflow, including driving frequency setting, data acquisition, and final data processing, was managed through custom MATLAB[1] code. The PC controlled the impedance analyzer via the IEEE-488 communication protocol, enabling fully automated frequency sweeps. The acquired impedance data were stored locally and subsequently processed in the MATLAB environment, where additional postprocessing was performed to evaluate the accuracy and repeatability of the proposed estimation methodology. Finally, each test was repeated ten times and the processed results were statistically analyzed to evaluate the robustness and the suitability of the proposed solution.

B. The Measurement Procedure

The measurement procedure consists of two main steps divided into elementary tasks, as shown in Fig. 6.

The first step is made offline and consist of three main tasks.

1) *Parameters Definition:* This task involves defining the characteristics of both the sample under test (SUT) and the ECP. Specifically, geometry, dimensions and physical parameters of the ECP, ranges of interest for both the electrical conductivity, lift-off and thickness, and range of interest for the driving frequency are established. The selection of SUT parameters is typically guided by prior knowledge of the materials to be tested, application-specific constraints (e.g., known materials or coatings ranges), and the driving frequency range that ensures skin depths suitable for the application. These constraints help to define realistic and physically

[1]Trademarked.

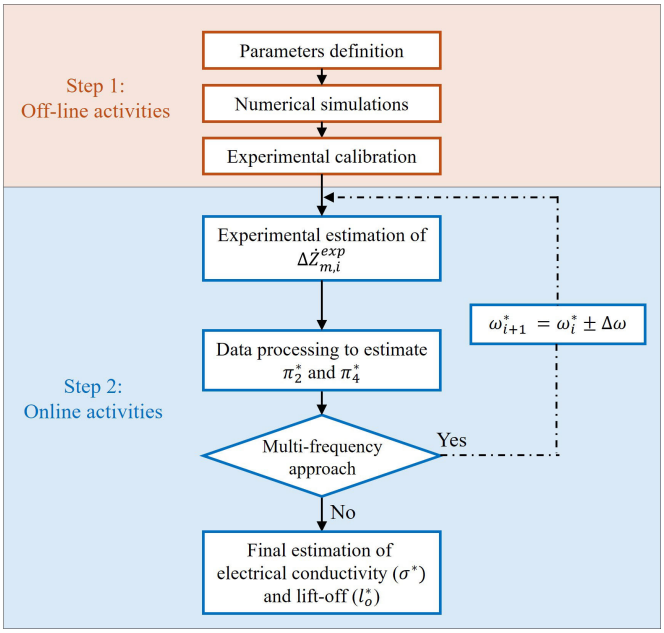

Fig. 6. Flowchart of the measurement procedure.

meaningful parameter intervals for both simulations and measurements.

2) *Numerical Simulations:* The evaluation of $\Delta\dot{Z}_m$ is performed using a simulation tool. In this article, the semi-analytical model proposed by Dodd and Deeds [26] has been used. The dimensionless parameter π_2, π_3, and π_4 are computed within the predefined range of interest as previously outlined in Table II.
3) *Experimental Calibration:* This task allows to find calibration factors to be used to match the simulated and measured features of $\Delta\dot{Z}_m$. Discrepancies may arise due to various factors such as model-specific assumptions, uncertainties in the knowledge of ECP geometry and material properties, experimental noise, measurement uncertainties, and so on. Using a reference plate with known electrical conductivity and thickness and considering a known lift-off value, a calibration factor for each driving frequency was obtained $c(f)$ as the ratio between numerically computed and experimentally measured data.

Since this first step is probe-dependent and establishes the ranges of interest for electrical conductivity, lift-off, thickness, and driving frequency, it is performed only once.

The second step is conducted online and involves three main tasks.

1) *Experimental Estimation of* $\Delta\dot{Z}_{m,i}^{\text{exp}}$*:* This task consists in experimentally measuring the mutual-impedances $\Delta\dot{Z}_{m,i}^{\text{exp}}$, at the ith prescribed driving frequency f_i. The value of f_i is selected from the range defined in the *parameters definition* task. The test may be performed at a single frequency or repeated at multiple frequencies to enhance the accuracy of the electrical conductivity and lift-off estimation.
2) *Data Processing to Estimate* π_2^* *and* π_4^**:* First, the calibration factor, at the ith driving frequency f_i, $c(f_i)$ is applied to the mutual impedance $\Delta\dot{Z}_{m,i}^{\text{exp}}$. Then, the corresponding dimensionless quantity $\bar{\pi}_{1,i}^{\text{exp}}$ is evaluated together with the corresponding level curves for $\text{Re}\{\bar{\pi}_{1,i}^{\text{exp}}\}$, $\text{Im}\{\bar{\pi}_{1,i}^{\text{exp}}\}$, $|\bar{\pi}_{1,i}^{\text{exp}}|$, and $\angle\bar{\pi}_{1,i}^{\text{exp}}$, and the intersection point $(\pi_{2,i}^*, \pi_{4,i}^*)$ among the level curves is determined, as shown in Fig. 3 (single-frequency approach) or Fig. 4 (multiple-frequency approach).
3) *Final Estimation of the Electrical Conductivity and Lift-Off:* The electrical conductivity $(\sigma_{,i}^*)$ and lift-off $(l_{o,i}^*)$ are estimated using (4) and (5), based on the intersection point $(\pi_{2,i}^*, \pi_{4,i}^*)$ obtained at the selected driving frequency in the previous task. If a multifrequency approach is employed, the final values of σ^* and l_o^* are determined as the average of those obtained at different driving frequencies.

IV. Results and Discussion

This section describes the obtained experimental results using the setup detailed in Section III-A and the procedure outlined in Section III-B. As already defined in Section III-A, the tests have been carried out by analyzing a range of driving frequencies spanning from 50 to 70 kHz. The sample M_8 was used for the experimental calibration process adopting the minimum lift-off (i.e., lo_1) configuration.

The results presentation begins showing the double estimation performance of the proposed method applying the single-frequency and single-measurement strategy. In this case, each test was carried out only once, without repetitions, and the aim is to demonstrate the effectiveness of the method under minimal measurement time to be applied for real-time inline inspections. To test the performance of the method with respect of the selected driving frequency, the single-frequency procedure was repeated for different frequencies in the defined range. For each driving frequency, the absolute relative errors in estimating electrical conductivity and lift-off were computed using the following expressions:

$$\varepsilon_{\sigma_i} = \frac{|\sigma_{e,i} - \sigma_a|}{\sigma_a} \cdot 100, \quad \varepsilon_{\text{lo}_i} = \frac{|\text{lo}_{e,i} - \text{lo}_a|}{\text{lo}_a} \cdot 100 \tag{6}$$

where $\sigma_{e,i}$ and $\text{lo}_{e,i}$ are the estimated electrical conductivity and lift-off at the ith driving frequency, respectively, and σ_a and lo_a are the known reference values.

The results are reported in Fig. 7, which shows the estimated absolute relative errors ε_{σ_i} and $\varepsilon_{\text{lo}_i}$ for all considered frequencies, materials and lift-off conditions.

Regarding the electrical conductivity, the analysis indicates that, in most cases, the error remains below 2%, thereby confirming the effectiveness of the method over the investigated frequency range. Only a limited number of cases exhibit an absolute relative error exceeding 2% (and never surpassing 4%), mostly observed at lower driving frequencies (i.e., between 50 and 60 kHz), where the EC response decreases and the sensitivity to electrical conductivity variations becomes weaker. Higher errors are also observed for greater lift-off values, where the increased distance between the probe and the sample decreases the magnetic coupling and reduces the

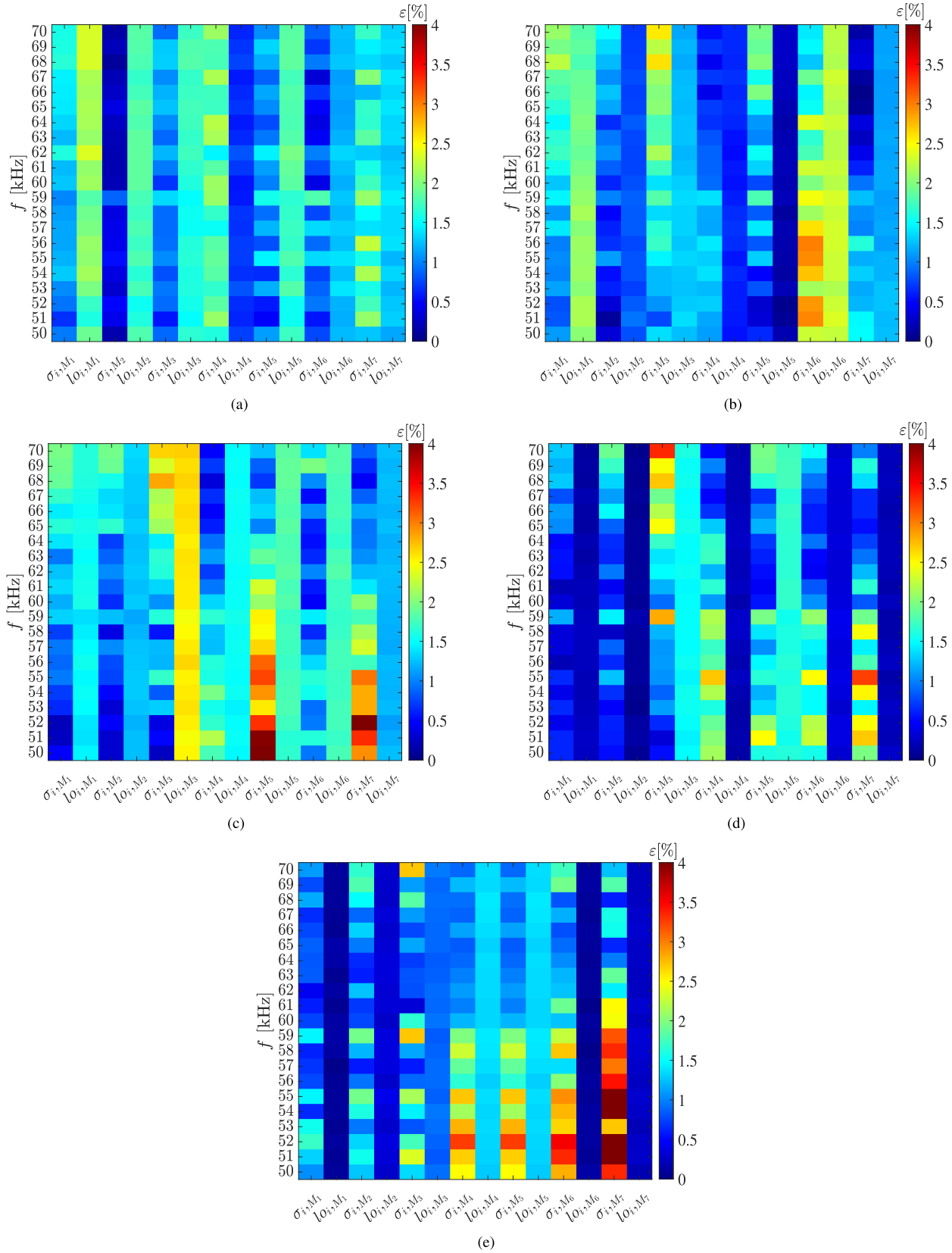

Fig. 7. Estimated absolute relative error at the ith frequency for electrical conductivity (ε_{σ_i}) and lift-off ($\varepsilon_{\mathrm{lo}_i}$) for all the considered materials at different lift-off conditions (a) lo_1, (b) lo_2, (c) lo_3, (d) lo_4, and (e) lo_5.

signal-to-noise ratio, thus affecting the estimation accuracy. In contrast, the lift-off estimation shows consistently superior performance. The absolute relative error remains below 2% under almost all test conditions and never exceeds 2.7%.

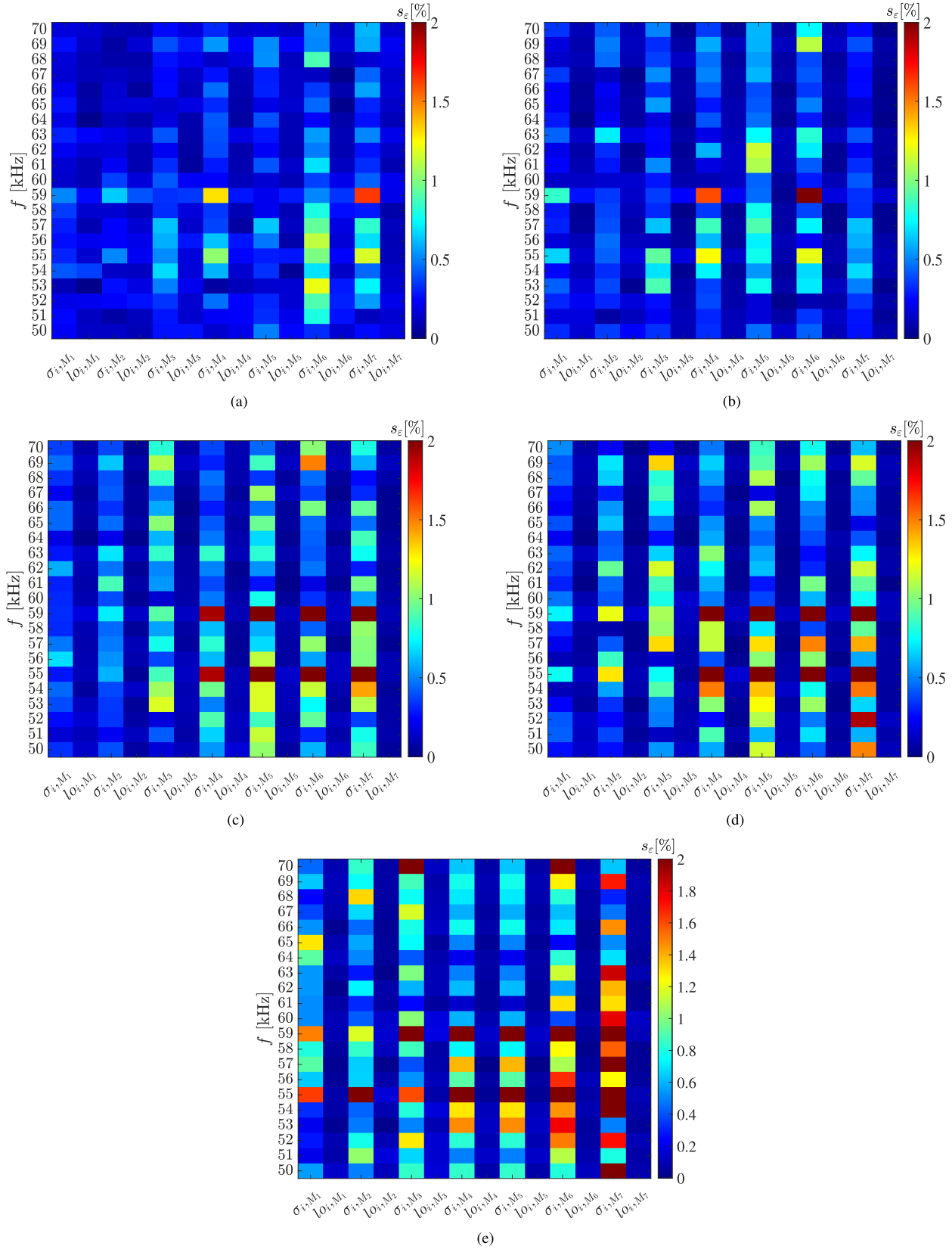

Fig. 8. Standard deviation of the absolute relative errors at the ith frequency for electrical conductivity ($s_{\varepsilon_{\sigma_i}}$) and lift-off ($s_{\varepsilon_{\mathrm{lo}_i}}$) for all the considered materials at different lift-off conditions (a) lo_1, (b) lo_2, (c) lo_3, (d) lo_4, and (e) lo_5.

Moreover, the performance is essentially independent of the selected driving frequency. This demonstrates that the proposed method is highly suitable for accurate lift-off reconstruction, even in configurations characterized by larger lift-off

TABLE VI

MEAN ABSOLUTE RELATIVE ERROR OF ELECTRICAL CONDUCTIVITY (ε_σ) AND LIFT-OFF ($\varepsilon_{\mathrm{lo}}$) OBTAINED WITH THE MULTIFREQUENCY STRATEGY USING ALL THE CONSIDERED FEATURES FOR LEVEL-CURVE INTERSECTION, FOR ALL SAMPLES AND LIFT-OFF CONFIGURATIONS

	lo_1		lo_2		lo_3		lo_4		lo_5	
	ε_σ [%]	ε_{lo} [%]	ε_σ [%]	ε_{lo} [%]	ε_σ [%]	ε_{lo} [%]	ε_σ [%]	ε_{lo} [%]	ε_σ [%]	ε_{lo} [%]
M_1	1.29	2.06	1.45	2.01	1.11	1.28	0.57	0.57	0.76	0.46
M_2	0.15	1.76	0.81	0.81	0.82	1.03	0.68	0.47	0.78	0.84
M_3	0.93	1.62	1.74	1.28	1.32	2.33	1.37	1.14	0.89	0.37
M_4	1.84	0.66	0.77	0.63	1.08	1.75	1.42	0.59	1.41	1.86
M_5	0.97	1.74	1.21	0.18	2.17	1.54	1.17	1.27	1.80	0.89
M_6	1.09	1.12	2.06	2.28	1.88	1.52	2.26	0.73	2.82	0.41
M_7	2.11	1.35	0.79	1.16	2.06	0.97	1.77	0.17	2.55	0.78

values or reduced excitation levels. In general, these findings support the effectiveness of the method in a single-frequency configuration.

It is important to note that the maximum tested lift-off (i.e., 2.27 mm) was selected to match typical nonconductive coating thicknesses in industrial practice. In our experience, these coatings typically do not exceed approximately 2 mm; hence, the chosen range is representative of the intended industrial use-case [8]. For larger lift-offs, the proposed inversion method remains applicable. However, because the interaction between the probe and the specimen decays rapidly with the lift-off, after a certain distance ($\pi_4 \gg 1$), the probe is insensitive to the plate within the noise level of the measurement instrument, that is, $\bar{\pi}_1 = G(\pi_2, \pi_4) \approx$ constant. This is a general limitation of all the measurement methods based on ECT. However, the interaction between the probe and the specimen can be improved by increasing the operating frequency and/or the amplitude of the driving current, and by replacing the probe with a larger one, that is, reducing π_4.

To evaluate the repeatability of the method, the measurements were repeated ten times for each frequency and configuration. In this case, the standard deviation of the absolute relative errors was calculated using

$$s_{\varepsilon_{\sigma_i}} = \sqrt{\frac{\sum_{j=1}^{N_t}\left(\varepsilon_{\sigma_{ij}} - \sum_{j=1}^{N_t}\varepsilon_{\sigma_{ij}}/N_t\right)^2}{N_t - 1}}$$
$$s_{\varepsilon_{\mathrm{lo}_i}} = \sqrt{\frac{\sum_{j=1}^{N_t}\left(\varepsilon_{\mathrm{lo}_{ij}} - \sum_{j=1}^{N_t}\varepsilon_{\mathrm{lo}_{ij}}/N_t\right)^2}{N_t - 1}} \quad (7)$$

where N_t is the number of repeated tests, and $\varepsilon_{\sigma_{ij}}$ and $\varepsilon_{\mathrm{lo}_{ij}}$ represent the relative errors at the ith frequency and jth repetition for electrical conductivity and lift-off, respectively.

The results of this analysis are shown in Fig. 8. The standard deviations of the relative errors remain below 1.5% and 0.17% for electrical conductivity and lift-off, respectively. Only few exceptions occurring at some specific driving frequencies (e.g. 54, 55, and 59 kHz) where, for the electrical conductivity, a slight increase in variability is observed (never exceeding 2%). Also, the results related to the repeatability confirm the goodness of the proposed method.

These results suggest that the observed variability is not an intrinsic limitation of the methodology, but rather the consequence of experimental conditions, most likely related to the specific characteristics of the measurement setup, such as the impedance analyzer and the signal-to-noise ratio at certain driving frequencies. Finally, it is confirmed the suitability of the application of the single-frequency solution, especially choosing driving frequencies greater than 60 kHz confirming the possibility to achieve highly repeatable and accurate parameter estimation with minimal measurement effort.

A second analysis has been carried out to evaluate the performance of the proposed method using the multifrequency strategy. This strategy is particularly advantageous in scenarios where optimal driving frequency range to select the single test frequency is not known a priori. The results of the measurements across all driving frequencies were aggregated. The mean absolute relative errors ε_σ and $\varepsilon_{\mathrm{lo}}$ were computed using

$$\varepsilon_\sigma = \frac{1}{N_f}\sum_{i=1}^{N_f}\varepsilon_{\sigma_i}, \quad \varepsilon_{\mathrm{lo}} = \frac{1}{N_f}\sum_{i=1}^{N_f}\varepsilon_{\mathrm{lo}_i}. \quad (8)$$

The results are summarized in Table VI that shows the mean absolute relative errors for each sample and lift-off configuration.

The reported results highlight as the performance in the lift-off estimation are the same of the single frequency strategy with a maximum mean absolute relative error always lower than 2.33% confirming the insensitivity of the lift-off estimation respect to the selected driving frequency. As far as the electrical conductivity estimation, the performance are overall better with mean absolute relative error generally lower than 1.5% and never greater than 2.82%. This confirms the robustness of the method across a broad range of physical conditions. The proposed method demonstrates better accuracy in the multifrequency strategy, ensuring high flexibility and adaptability to various inspection scenarios and user constraints.

A further analysis was carried out to assess the impact of the selected feature set on the estimation performance. Specifically, the proposed method was tested both in the single-frequency configuration and in the multifrequency strategy by using the minimum number of features required to solve the inverse problem (i.e., two features), rather than exploiting all the available features. Two feature pairs were considered for the level-curve intersection: the real and imaginary parts of $\bar{\pi}_1$ (i.e., $\mathrm{Re}\{\bar{\pi}_1\}$–$\mathrm{Im}\{\bar{\pi}_1\}$) and the magnitude and phase of $\bar{\pi}_1$ (i.e., $|\bar{\pi}_1|$–$\angle\bar{\pi}_1$). The performed analysis showed very similar trends and conclusions for both single-frequency and multifrequency implementations. For conciseness, in the

TABLE VII

MEAN ABSOLUTE RELATIVE ERROR OF ELECTRICAL CONDUCTIVITY (ε_σ) AND LIFT-OFF (ε_{LO}) OBTAINED USING THE MULTIFREQUENCY STRATEGY AND THE RE$\{\bar{\pi}_1\}$–IM$\{\bar{\pi}_1\}$ FEATURE COMBINATION FOR LEVEL-CURVE INTERSECTION, FOR ALL SAMPLES AND LIFT-OFF CONFIGURATIONS

	lo_1		lo_2		lo_3		lo_4		lo_5	
	ε_σ [%]	ε_{lo} [%]	ε_σ [%]	ε_{lo} [%]	ε_σ [%]	ε_{lo} [%]	ε_σ [%]	ε_{lo} [%]	ε_σ [%]	ε_{lo} [%]
M_1	1.29	2.06	1.45	2.01	1.11	1.28	0.57	0.56	0.76	0.46
M_2	0.15	1.76	0.81	0.81	0.82	1.03	0.69	0.45	0.78	0.84
M_3	0.94	1.62	1.64	1.28	1.31	2.33	1.43	1.15	0.89	0.37
M_4	1.86	0.68	0.81	0.60	1.12	1.74	1.44	0.60	1.45	1.82
M_5	0.97	1.74	1.17	0.18	2.17	1.54	1.17	1.29	1.79	0.89
M_6	1.09	1.23	2.15	2.26	2.02	1.53	2.38	0.73	2.80	0.41
M_7	2.11	1.32	0.56	1.21	2.04	0.99	1.67	0.14	2.78	0.77

TABLE VIII

MEAN ABSOLUTE RELATIVE ERROR OF ELECTRICAL CONDUCTIVITY (ε_σ) AND LIFT-OFF (ε_{LO}) OBTAINED USING THE MULTIFREQUENCY STRATEGY AND THE $|\bar{\pi}_1|$–$\angle\bar{\pi}_1$ FEATURE COMBINATION FOR LEVEL-CURVE INTERSECTION, FOR ALL SAMPLES AND LIFT-OFF CONFIGURATIONS

	lo_1		lo_2		lo_3		lo_4		lo_5	
	ε_σ [%]	ε_{lo} [%]	ε_σ [%]	ε_{lo} [%]	ε_σ [%]	ε_{lo} [%]	ε_σ [%]	ε_{lo} [%]	ε_σ [%]	ε_{lo} [%]
M_1	1.26	2.07	1.42	2.00	1.05	1.29	0.55	0.56	0.75	0.44
M_2	0.14	1.77	0.77	0.80	0.81	1.04	0.67	0.45	0.86	0.83
M_3	0.96	1.66	1.66	1.26	1.27	2.35	1.39	1.15	0.92	0.40
M_4	1.86	0.67	0.80	0.62	1.13	1.74	1.42	0.60	1.43	1.85
M_5	0.98	1.77	1.11	0.19	2.19	1.56	1.19	1.29	1.91	0.90
M_6	1.12	1.20	2.06	2.28	1.97	1.52	2.25	0.73	2.82	0.41
M_7	2.10	1.31	0.54	1.24	2.06	0.98	1.69	0.14	2.68	0.78

TABLE IX

COMPARISON BETWEEN THE PROPOSED METHOD AND REPRESENTATIVE APPROACHES FROM THE SCIENTIFIC LITERATURE

Method	Approach	Electrical conductivity range [MS/m]	Lift-off range [mm]	$\bar{\varepsilon}_\sigma$ [%]	$\bar{\varepsilon}_{lo}$ [%]	Estimation time [s]
Rodrigues *et al.* [4]	Single frequency	4.95 - 60.48	0 - 0.6	1.18	4.36	36
Lu *et al.* [17]	Multiple frequencies	3.37 - 4.13	1.0 - 20.0	2.95	6.30	N/A
Lee *et al.* [18]	Multiple frequencies	0.56 - 1.92	1 - 5	1.04	1.21	N/A
Huang *et al.* [19]	Multiple frequencies	0.53 - 62.1	1 - 5	3.50	1.00	30.3
Proposed method (four-features configuration)	Single frequency	5.28 - 58.05	0.41 - 2.27	1.41	1.21	0.45
	Multiple frequencies			1.36	1.13	9.41
Proposed method (pair-features configuration)	Single frequency	5.28 - 58.05	0.41 - 2.27	1.43	1.22	0.15
	Multiple frequencies			1.38	1.14	3.08

following, we report only the results obtained with the multifrequency strategy. The corresponding mean absolute relative errors for electrical conductivity and lift-off adopting the Re$\{\bar{\pi}_1\}$–Im$\{\bar{\pi}_1\}$ and the $|\bar{\pi}_1|$–$\angle\bar{\pi}_1$ feature combinations are reported in Tables VII and VIII, respectively. The results show that limiting the estimation process to two features does not significantly degrade the method's performance compared to using all available features. Depending on the material and lift-off condition, slightly better performance can be observed when using either all features or a feature pair. Most importantly, the maximum discrepancy among the obtained mean errors is consistently below 0.2%, confirming the robustness of the proposed estimation framework with respect to the choice of feature set.

To demonstrate the computational efficiency of the proposed approach, an analysis of the estimation time of the online activities was carried out. In particular, the analysis focused on the operations related to the "data processing to estimate π_2^* and π_4^*" and to the "final estimation of electrical conductivity and lift-off" as described in Section III-B. The estimation time was measured using a standard laptop equipped with an Intel[2] i5-8250 processor and 32 GB RAM. Two operational configurations were evaluated: 1) the single-frequency approach, in which the estimation process is performed at one selected driving frequency; and 2) the multifrequency approach, in which all 21 driving frequencies from 50 to 70 kHz are processed, with a step of 1 kHz. The reported computational times refer to the four-features configuration, that is, when the level-curve intersection exploits all four features of $\bar{\pi}_1$ (Re$\{\bar{\pi}_1\}$, Im$\{\bar{\pi}_1\}$, $|\bar{\pi}_1|$, and $\angle\bar{\pi}_1$). In this case, the estimation time was approximately 0.45 s for the single-frequency approach and about 9.41 s for the multifrequency approach. When only one feature pair is used for inversion (e.g., Re$\{\bar{\pi}_1\}$–Im$\{\bar{\pi}_1\}$ or $|\bar{\pi}_1|$–$\angle\bar{\pi}_1$), the computational effort further decreases, leading to estimation times of approximately 0.15 s for the single-frequency approach and 3.08 s for the multifrequency approach. Overall, the proposed method proves suitable for real-time and inline applications, achieving

[2]Registered trademark.

subsecond estimation in the single-frequency configuration and processing times well below 10 s even in the most demanding multifrequency case, on a standard laptop and without hardware acceleration or parallel computing. Moreover, an alternative hardware implementation based on the Cyclone V 5CSXFC6D6F31C6N FPGA [29], used in [30] for the simultaneous estimation of thickness and electrical conductivity [22], achieved an estimation time of approximately 800 μs for a single-frequency approach, considering the same processing stages.

Finally, Table IX provides a comparison between the proposed approach and representative methods available in the literature [4], [17], [18], [19]. For each method, the analyzed range of electrical conductivity and lift-off, the corresponding mean estimation errors ($\overline{\varepsilon}_\sigma$, $\overline{\varepsilon}_{\text{lo}}$), and the estimation time are reported. The proposed method achieves accuracy comparable to or better than state-of-the-art approaches, while reducing computational cost. Unlike most existing methods, often relying on multifrequency acquisition and iterative or data-driven inversion approach, the proposed method provides accurate and repeatable estimations from single-frequency and multifrequency excitation.

V. Conclusion

In this article, a novel methodology is proposed for the simultaneous estimation of electrical conductivity and lift-off in ECT, using either a single or multifrequency strategy. It is based on the application of a dimensional analysis approach using Buckingham's ptheorem that reduces the complexity of the problem by bringing the estimation process into a smaller dimensionless space. The proposed approach does not require any approximation of the underlying model, making it robust against large variations in electrical conductivity and lift-off. Experimental validation was performed on various conductive samples with electrical conductivities between 5.28 and 58.05 MS/m and lift-off values between 0.41 and 2.27 mm. The results obtained showed good accuracy and repeatability, with mean absolute relative errors less than 3% for electrical conductivity and 2% for lift-off. A major benefit of the proposed technique is its suitability for single-frequency operation, which significantly reduces the measurement time and makes it highly applicable to real-time and online industrial test scenarios. Unlike multifrequency and sweep-frequency approaches, which require longer acquisition times, the proposed method provides fast and accurate estimations while maintaining robustness. In addition, the proposed inversion can be performed either by exploiting all four features of $\bar{\pi}_1$ (Re$\{\bar{\pi}_1\}$, Im$\{\bar{\pi}_1\}$, $|\bar{\pi}_1|$, and $\angle\bar{\pi}_1$) to maximize robustness, or by using only one feature pair (e.g., Re$\{\bar{\pi}_1\}$–Im$\{\bar{\pi}_1\}$ or $|\bar{\pi}_1|$–$\angle\bar{\pi}_1$) to further reduce computational time, with negligible impact on accuracy. While the proposed method has been developed and validated for nonmagnetic materials, future efforts will target its extension to magnetic materials, where additional dimensionless parameters related to magnetic permeability must be considered. Future work will also include a metrological characterization of the method to quantify sources of error, determine optimal excitation frequencies, and select the best combination of features (number and typology) based on the unknown values of the quantity to be estimated, in order to improve accuracy and sensitivity. This work also opens the way to extending the methodology toward triple-parameter estimation (e.g., thickness, lift-off, and electrical conductivity).

TABLE X
Dimensional Variables Involved in the ECT Problem Description, Expressed in Terms of Fundamental Dimensions

Parameters	Symbols	Fundamental dimensions
q_1	$\Delta\dot{Z}_m$	$[L^0T^0\Omega^1]$
q_2	σ	$[L^{-1}T^0\Omega^{-1}]$
q_3	ν_0	$[L^1T^{-1}\Omega^{-1}]$
q_4	ω	$[L^0T^{-1}\Omega^0]$
q_5	Δh	$[L^1T^0\Omega^0]$
q_6	l_0	$[L^1T^0\Omega^0]$
q_7	D	$[L^1T^0\Omega^0]$
q_8	$\mathbf{t}$	$[L^0T^0\Omega^0]$
q_9	θ	$[L^0T^0\Omega^0]$

Appendix

A. Buckingham's π Theorem Application to the ECT Problem

For the convenience of the reader, this appendix briefly recalls the methodology described in [22] for deriving the dimensionless formulation of the ECT problem.

The starting point is (1), which specifies the dependence of the measured quantity from its influencing parameters q_i's, listed in Table X.

The aim is to rewrite (1) in terms of dimensionless quantities only, called π-groups and denoted by π_i's. Each of the π-groups is a combination of the physical quantities q_i appearing in (1) and, hence, can be written as [20]

$$\pi_i = q_1^{\alpha_{i1}} \dots q_j^{\alpha_{ij}} \dots q_n^{\alpha_{in}}.$$

Following the procedure outlined in [22] and [31], the exponents α_{ij} are determined by identifying a set of k "repeating variables" among the n physical quantities $q_1, \dots, q_n$. These variables are the ones appearing in each $\pi-$groups. The repeating variables need to satisfy the following constraints: 1) when multiplied, with proper exponents, it is possible to obtain all the physical dimensions needed to describe the problem, that is, Ω, L and T; 2) they are independent; 3) their nontrivial products cannot provide dimensionless quantities; and 4) they are not dependent variable of the problem ($\Delta\dot{Z}$ in this case).

A possible choice for the repeating variables is the set $\{D, \omega, \nu_0\}$, which fulfills the four conditions stated above. Accordingly, the π-groups for the ECT problem can be expressed as

$$\pi_i = D^{\alpha_{1i}} \omega^{\alpha_{2i}} \nu_0^{\alpha_{3i}} q_{3+i}, \quad i = 1, \dots, n-3$$

where each dimensionless group is obtained by introducing one of the remaining dimensional variables at a time.

Finally, the unknown coefficients are determined by imposing that the π_i's are dimensionless. For example, π_1 is determined starting from

$$\bar{\pi}_1 = D^{\alpha_{11}} \omega^{\alpha_{21}} \nu_0^{\alpha_{31}} \Delta\dot{Z}$$

resulting in the following system of equations (see Table X):

$$\begin{cases} 0 = \alpha_{11} + \alpha_{31} \\ 0 = -\alpha_{21} - \alpha_{31} \\ 0 = -\alpha_{31} + 1 \end{cases}$$

whose solution is

$$\begin{cases} \alpha_{11} = -1 \\ \alpha_{21} = -1 \\ \alpha_{31} = 1. \end{cases}$$

ACKNOWLEDGMENT

This study was carried out within the MOST - Sustainable Mobility Center and received funding from the European Union Next-GenerationEU (PIANO NAZIONALE DI RIPRESA E RESILIENZA (PNRR) - MISSIONE 4 COMPONENTE 2, INVESTIMENTO 1.4 - D.D. 1033 17/06/2022, CN00000023). This manuscript reflects only the authors' views and opinions, neither the European Union nor the European Commission can be considered responsible for them.

REFERENCES

[1] M. Dimitrova, A. Aminzadeh, M. S. Meiabadi, S. Sattarpanah Karganroudi, H. Taheri, and H. Ibrahim, "A survey on non-destructive smart inspection of wind turbine blades based on industry 4.0 strategy," *Appl. Mech.*, vol. 3, no. 4, pp. 1299–1326, Nov. 2022.

[2] J. Lario, J. Mateos, F. Psarommatis, and Á. Ortiz, "Towards zero defect and zero waste manufacturing by implementing non-destructive inspection technologies," *J. Manuf. Mater. Process.*, vol. 9, no. 2, p. 29, Jan. 2025.

[3] V. Medici et al., "Integration of non-destructive inspection (NDI) systems for zero-defect manufacturing in the industry 4.0 era," in *Proc. IEEE Int. Workshop Metrol. Ind. 4.0 IoT*, Jun. 2023, pp. 439–444.

[4] N. M. Rodrigues, L. S. Rosado, and P. M. Ramos, "A portable embedded contactless system for the measurement of metallic material conductivity and lift-off," *Measurement*, vol. 111, pp. 441–450, Dec. 2017.

[5] C. Wang, M. Fan, B. Cao, B. Ye, and W. Li, "Novel noncontact eddy current measurement of electrical conductivity," *IEEE Sensors J.*, vol. 18, no. 22, pp. 9352–9359, Nov. 2018.

[6] G. Betta, L. Ferrigno, M. Laracca, A. Rasile, and A. Sardellitti, "Thickness measurements with eddy current and ultrasonic techniques," in *Sensors and Microsystems*. Cham, Switzerland: Springer, 2020, pp. 387–394.

[7] F. Carere, A. Sardellitti, A. Bernieri, L. Ferrigno, S. Sangiovanni, and M. Laracca, "An eddy current probe for the detection of subsuperficial defects of any orientation," *IEEE Trans. Instrum. Meas.*, vol. 73, pp. 1–13, 2024.

[8] A. Sardellitti, F. Milano, M. Laracca, L. Ferrigno, A. Tamburrino, and G. Y. Tian, "Enhancing corrosion detection and characterization: An innovative approach with pot-cored eddy current probe," *IEEE Trans. Instrum. Meas.*, vol. 74, pp. 1–13, 2025.

[9] A. Celzard, J. F. Mareché, F. Payot, D. Bégin, and G. Furdin, "Electrical conductivity of anthracites as a function of heat treatment temperature," *Carbon*, vol. 38, no. 8, pp. 1207–1215, 2000.

[10] S. B. Pankade, D. S. Khedekar, and C. L. Gogte, "The influence of heat treatments on electrical conductivity and corrosion performance of AA 7075-T6 aluminium alloy," *Proc. Manuf.*, vol. 20, pp. 53–58, Jan. 2018.

[11] Q. Zhao et al., "Review on the electrical resistance/conductivity of carbon fiber reinforced polymer," *Appl. Sci.*, vol. 9, no. 11, p. 2390, Jun. 2019.

[12] P. Huang, Z. Li, J. Long, L. Xu, and Y. Xie, "Measurement of lift-off distance and thickness of nonmagnetic metallic plate using pulsed eddy current testing," *IEEE Trans. Instrum. Meas.*, vol. 72, pp. 1–10, 2023.

[13] J. Li, X. Wu, Q. Zhang, and P. Sun, "Measurement of lift-off using the relative variation of magnetic flux in pulsed eddy current testing," *NDT E Int.*, vol. 75, pp. 57–64, Oct. 2015.

[14] L. Dziczkowski, "Elimination of coil liftoff from eddy current measurements of conductivity," *IEEE Trans. Instrum. Meas.*, vol. 62, no. 12, pp. 3301–3307, Dec. 2013.

[15] W. Chen and D. Wu, "Resistance-frequency eddy current method for electrical conductivity measurement," *Measurement*, vol. 209, Mar. 2023, Art. no. 112501.

[16] Y. Xie, P. Huang, Y. Ding, J. Li, H. Pu, and L. Xu, "A novel conductivity measurement method for non-magnetic materials based on sweep-frequency eddy current method," *IEEE Trans. Instrum. Meas.*, vol. 71, pp. 1–12, 2022.

[17] M. Lu, X. Meng, R. Huang, L. Chen, A. Peyton, and W. Yin, "Measuring lift-off distance and electromagnetic property of metal using dual-frequency linearity feature," *IEEE Trans. Instrum. Meas.*, vol. 70, pp. 1–9, 2021.

[18] K.-M. Lee, C.-Y. Lin, B. Hao, and M. Li, "Coupled parametric effects on magnetic fields of eddy-current induced in non-ferrous metal plate for simultaneous estimation of geometrical parameters and electrical conductivity," *IEEE Trans. Magn.*, vol. 53, no. 10, pp. 1–9, Oct. 2017.

[19] P. Huang et al., "Decoupling permeability, conductivity, thickness, lift-off for eddy current testing using machine learning," *IEEE Trans. Instrum. Meas.*, vol. 72, pp. 1–10, 2023.

[20] E. Buckingham, "On physically similar systems; illustrations of the use of dimensional equations," *Phys. Rev.*, vol. 4, no. 4, pp. 345–376, Oct. 1914.

[21] A. Sardellitti et al., "Metrological characterization of an ECT method for thickness estimation based on dimensional analysis," in *Proc. IEEE 10th Int. Workshop Metrology Aerosp. (MetroAeroSpace)*, Jun. 2023, pp. 441–446.

[22] A. Tamburrino, A. Sardellitti, F. Milano, V. Mottola, M. Laracca, and L. Ferrigno, "Old but not obsolete: Dimensional analysis in nondestructive testing and evaluation," *NDT E Int.*, vol. 141, Jan. 2024, Art. no. 102977.

[23] A. Sardellitti, V. Mottola, F. Milano, L. Ferrigno, A. Tamburrino, and M. Laracca, "Simultaneous estimation of conductivity and lift-off using dimensional analysis: A preliminary analysis," in *Proc. 11th Int. Workshop Metrology Aerosp. (MetroAeroSpace)*, Jun. 2024, pp. 106–111.

[24] H. Wang, W. Li, and Z. Feng, "Noncontact thickness measurement of metal films using eddy-current sensors immune to distance variation," *IEEE Trans. Instrum. Meas.*, vol. 64, no. 9, pp. 2557–2564, Sep. 2015.

[25] C.-Y. Lin, Y.-C. Wu, and M. Teng, "Development of a magnetic eddy-current sensing system for simultaneous estimation of electrical conductivity and thickness in non-ferrous metal plates," *IEEE/ASME Trans. Mechatronics*, vol. 28, no. 1, pp. 360–371, Jan. 2022.

[26] C. V. Dodd and W. E. Deeds, "Analytical solutions to eddy-current probe-coil problems," *J. Appl. Phys.*, vol. 39, no. 6, pp. 2829–2838, May 1968.

[27] . Accessed: Oct. 9, 2025. [Online]. Available: https://www.gwinstek.com/en-global/products/detail/LCR-8000G

[28] *Sigmacheck 2*. Accessed: Dec. 18, 2025. [Online]. Available: https://ethernde.com/products/conductivity-meters/sigmacheck-2

[29] *Cyclone V 5CSXC6 FPGA*. Accessed: Dec. 18, 2025. [Online]. Available: https://www.intel.com/content/www/us/en/products/sku/210462/cyclone-v-5csxc6-fpga/specifications.html

[30] L. Ferrigno, V. Mottola, S. Palazzo, A. Sanseverino, A. Sardellitti, and A. Tamburrino, "Dimensional analysis and fpga-based implementation for real-time thickness and conductivity estimation in eddy current testing," in *Proc. IEEE 29th Workshop Signal Power Integrity (SPI)*, May 2025, pp. 1–4.

[31] R. C. O. Tang et al., "Review on design factors of microbial fuel cells using Buckingham's pi theorem," *Renew. Sustain. Energy Rev.*, vol. 130, Sep. 2020, Art. no. 109878.

Alessandro Sardellitti (Member, IEEE) received the M.S. degree (summa cum laude) in electrical engineering and the Ph.D. degree in methods, models, and technologies for engineering from the University of Cassino and Southern Lazio, Cassino, Italy, in 2018 and 2024, respectively.

He is currently an Assistant Professor (RTT) of electrical and electronic measurements at the Faculty of Technological Sciences and Innovation, Universitas Mercatorum, Rome, Italy. His research interests include measurement methodologies, numerical modeling, and experimental techniques for nondestructive testing and evaluation (NDT&E), with a particular focus on eddy current testing. His work mainly concerns electromagnetic sensor design for defect detection and material characterization in industrial, aerospace, and civil engineering applications.

Vincenzo Mottola (Member, IEEE) received the M.S. degree (summa cum laude) in electrical engineering and the Ph.D. degree in methods, models, and technologies for engineering from the University of Cassino and Southern Lazio, Cassino, Italy, in 2021 and 2024, respectively.

He is currently a Research Fellow with the Department of Electrical and Information Engineering, University of Cassino and Southern Lazio. He is also active in computational electromagnetics, focusing on the development of models and numerical methods. His research interests include inverse problems and the development of real-time methods for electromagnetic tomography and nondestructive testing aimed at the characterization of linear and nonlinear materials.

Filippo Milano (Member, IEEE) received the M.S. degree (summa cum laude) in electrical engineering and the Ph.D. degree in methods, models, and technologies for engineering from the University of Cassino and Southern Lazio, Cassino, Italy, in 2018 and 2021, respectively.

He is currently a Research Fellow at the Department of Electrical and Information Engineering, University of Cassino and Southern Lazio. His research interests involve the design, implementation, and characterization of positioning systems for biomedical and industrial applications, the development of models and techniques for the predictive batteries diagnosis, and the application of eddy current techniques for the estimation of geometric and physical properties of conductive materials.

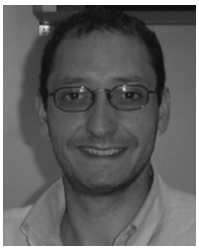

Marco Laracca (Member, IEEE) received the M.S. degree in electrical engineering and the Ph.D. degree in electrical and information engineering from the University of Cassino and Southern Lazio, Cassino, Italy, in 2002 and 2006, respectively.

Since 2021, he has been an Associate Professor of electrical and electronic measurements with the Sapienza University of Rome, Rome, Italy. His current research interests include the realization of the measurement system for nondestructive testing, sensor realization and characterization, and speed calibration.

Dr. Laracca is member of IEEE Instrumentation and Measurement Technical Committee-1 (TC-1) on "Nondestructive Evaluation and Industrial Inspection (NDE&II)."

Luigi Ferrigno (Senior Member, IEEE) is a Full Professor of electric and electronic measurement and the Vice-Rector for the third mission at the University of Cassino and Southern Lazio, Cassino, Italy. He coordinated and participated in several national and international research and technology transfer projects. His research interests include developing innovative and distributed measurement systems and methods for several application fields such as energy, sustainable mobility, NDT4.0, smart cities, the Internet of Things (IoT), and automotive.

Antonello Tamburrino (Senior Member, IEEE) received the Laurea degree (summa cum laude) in electronic engineering from the University of Naples Federico II, Naples, Italy, in 1992, and the Ph.D. degree in electronic engineering from the Polytechnic University of Turin, Turin, Italy, in 1996.

He joined the College of Engineering, University of Cassino and Southern Latium, Cassino, Italy, in 1994, where he served as an Assistant Professor from 1994 to 2001 and as an Associate Professor from 2001 to 2006. Since 2006, he has been a Full Professor of electrical engineering. From 2014 to 2018, he was also a Full Professor of electrical engineering at the College of Engineering, Michigan State University, East Lansing, MI, USA. He has authored or co-authored more than 250 papers in refereed international journals, books, and conference proceedings, and is a Co-Editor of three proceedings volumes. His current research interests include inverse problems, electromagnetic imaging, nondestructive evaluation, computational electromagnetism, plasmonics, and homogenization methods.

Dr. Tamburrino serves as the Editor-in-Chief for *International Journal on Applied Electromagnetics and Mechanics*, a Subject Editor for *NDT & E International*, and an Associate Editor for *Nondestructive Testing and Evaluation*.